Competing interactions in population-imbalanced two-component Bose-Einstein condensates

Peder Notto Galteland and Asle Sudbø
Department of Physics, NTNU, Norwegian University of Science and Technology, N-7491 Trondheim, Norway
(Received 24 June 2016; revised manuscript received 25 July 2016; published 15 August 2016)

We consider a two-component Bose-Einstein condensate with and without synthetic "spin-orbit" interactions in two dimensions. Density and phase fluctuations of the condensate are included, allowing us to study the impact of thermal fluctuations and density-density interactions on the physics originating with spin-orbit interactions. In the absence of spin-orbit interactions, we find that intercomponent density interactions deplete the minority condensate. The thermally driven phase transition is driven by coupled density and phase-fluctuations, but is nevertheless shown to be a phase-transition in the Kosterlitz-Thouless universality class with close to universal amplitude ratios irrespective of whether both the minority- and majority condensates exist in the ground state, or only one condensate exists. In the presence of spin-orbit interactions we observe three separate phases, depending on the strength of the spin-orbit coupling and intercomponent density-density interactions: a phase-modulated phase with uniform amplitudes for small intercomponent interactions, a completely imbalanced, effectively single-component condensate for intermediate spin-orbit coupling strength and sufficiently large intercomponent interactions, and a phase-modulated *and* amplitude-modulated phase for sufficiently large values of both the spin-orbit coupling and the intercomponent density-density interactions. The phase that is modulated by a single $\boldsymbol{q}$-vector only is observed to transition into an isotropic liquid through a strong depinning transition with periodic boundary conditions, which weakens with open boundaries.

DOI: 10.1103/PhysRevB.94.054510

I. INTRODUCTION

Spin-orbit coupling (SOC) underpins many fascinating phenomena in condensed-matter physics, including spin-Hall [1,2] effects and the existence of topological insulators [3–6]. SOC is also important for determining the physical properties of such important functional materials as GaAs [7]. Due to the fundamental magnetoelectric character of SOC in charged systems, it also has important ramifications for the manipulation of spin degrees of freedom using electric fields, currently a research topic of intense focus. While these examples represent systems in which a real physical spin is coupled to the orbital motion of electrons, similar phenomena may also be investigated in bosonic systems. Here, the SOC does not originate with a relativistic correction to the equations of motion, as it does in the electronic systems mentioned above. Rather, it is synthetic in the sense of being engineered [8,9], Rashba [10], and Dresselhaus [11] coupling in multicomponent Bose-Einstein condensates. Such multicomponent condensates could be either homonuclear, with different species occupying different hyperfine spin states [12,13], or they could be mixtures of different types of bosons [14,15]. In either case, one may associate an index with each species of the condensate, serving as an internal "spin" degree of freedom. A great advantage of studying the physics of competing interactions and couplings in Bose-Einstein condensates or other ultracold atomic systems is that the interaction parameters, namely density-density interactions and "spin-orbit" couplings, are highly tunable. This facilitates the study of a wide range of phenomena that are otherwise not accessible in standard condensed-matter systems.

SOC in a confined bosonic gas of cold atoms has been achieved using an optical Raman-dressing scheme [8]. A similar scheme has also been used in cold fermionic gases [16]. In optical lattices [17], synthetic SOC has been realized in a one-dimensional lattice using a similar Raman-dressing scheme [18]. Other proposals for realizing SOC in an optical lattice include periodically driving the lattice with an oscillating magnetic-field gradient [19], or using off-resonance laser beams [20]. The latter two schemes avoid the problem of heating caused by spontaneous emission of photons, as they do not rely on near-resonant laser fields.

In the case of topological insulators, the classification scheme and the physical properties of these systems are largely worked out and predicted at zero temperature and ignoring many-body interactions [6,21–23]. It seems worthwhile to examine the effects of both temperature and many-body interactions on the effect of SOC. In this respect, looking at "pseudospin" Bose-Einstein condensates offers an attractive alternative for studying many-body effects, since one can, among other things, perform large-scale Monte Carlo simulations without the complicating factors arising from Fermi statistics in the problem. Bosonic systems also have the attractive property of featuring a condensate at low enough temperatures, such that one has a mean-field starting point to compare with, at least provided the system is placed far enough away in parameter space from the critical point arising either from interaction effects or thermal fluctuations.

Previous works on bosonic spin-orbit coupled condensates have shown that their ground state has a periodically modulated striped spin structure both in a lattice model [24–27] and by considering the continuum Gross-Pitaevskii equations [28–30]. Including SOC splits the energy bands of spin-up and spin-down particles into bands of definite helicity, where the lower band will have minima at finite momentum, provided that any additional Zeeman splitting (i.e., imbalance in the condensate density) of the bands is not too large. A continuum model will have a degenerate ring of minima in momentum space, with a fixed length of the momentum vector in two dimensions, while a square lattice will break the degeneracy down to four points along the diagonals of the lattice. It has also been shown that, in the weak-coupling limit, the bosons will

condense either into one or two minima in the ground state, depending on the strength of the intracomponent interactions. Furthermore, the stability of the Rashba-coupled Bose gases in the presence of thermal and quantum fluctuations has been studied in the Bogoliubov approximation [31,32]. However, the full range of thermal fluctuations has not been considered before in such systems.

In this paper, therefore, we consider a two-dimensional two-component Bose-Einstein condensate with Rashba synthetic SOC. The condensates are also assumed to be population-imbalanced with different densities among the components in the ground state. Fluctuation effects are strong in two-dimensional systems such that no local order parameters exist for systems with continuous symmetries. Even so, one may get some rough insights into the effects of varying interactions and temperature at the mean-field level. For a spin-orbit coupled system featuring a nonuniform ground state, this differs from the case in which one expects a uniform ground state, in that the gradient terms of the theory need to be included even at the mean-field level. We will perform such a mean-field analysis in this paper, and we will compare the results to what we obtain in large-scale Monte Carlo simulations. At low temperatures, we find that a mean-field analysis yields results for critical values of interaction parameters that destroy the minority condensate, in good agreement with Monte Carlo simulations. At elevated temperatures, we find that the amplitude-fluctuating two-component condensate undergoes Kosterlitz-Thouless phase transitions for two qualitatively different parameter regimes. (i) In the absence of SOC, we find that the condensate loses phase coherence via proliferation of vortex-antivortex pairs in an amplitude-fluctuating background, and that this phase transition is a Kosterlitz-Thouless phase transition with a universal amplitude ratio of the jump in superfluid density to critical temperature given by $2/\pi$. (ii) In a parameter regime where SOC plays a role, and gives a nonuniform ground state in the form of stripes of modulated *phases* (but not amplitudes) of the condensate ordering fields, we find via finite-size scaling of the structure functions at the pseudo-Bragg vectors that the stripes melt through thermal depinning from the lattice, and not in a Kosterlitz-Thouless phase transition. When the condensate we study features a nonuniform ground state, it may be thought of as a bosonic analog to either a two-dimensional two-component superconductor in a Larkin-Ovchinnikov state, or to a one-component superconductor in a Fulde-Ferrell state. The former features topological order at finite temperature, the latter is topologically disordered at any finite temperature [33].

The paper is structured as follows. Section II presents the model and observables we use to classify the states and transitions observed. Section III contains the mean-field calculations. Section IV describes the Monte Carlo scheme we use. In Sec. Section V, all our Monte Carlo results as well as discussions on their significance are included. We present our conclusions in Sec. VI.

II. MODEL

In this section, we present the lattice model used in the Monte Carlo simulations, discuss some of its basic properties, and present the observables measured in simulations to classify the phases and phase transitions that we observe.

A. Ginzburg-Landau model

The starting point of our formulation is the standard two-component Ginzburg-Landau model with an added SOC, given by

$$H = \int d^2r \left[\frac{1}{2} |\nabla \Psi|^2 + V(\Psi) \right] + H_{\mathrm{SO}}. \tag{1}$$

Here, $\Psi^\dagger = (\psi_1^*, \psi_2^*)$ is a spinor of two complex fields, where the individual components may be thought of as a pseudospin degree of freedom, and V is the potential. We allow the potential to contain inter- and intracomponent density-density interactions, as well as a chemical potential. The chemical potential is chosen to have different strengths for each component, which may be viewed as a Zeeman-like field acting on the pseudospins,

$$V(\Psi) = \sum_i \alpha_i |\psi_i|^2 + \sum_{ij} g_{ij} |\psi_i|^2 |\psi_j|^2. \tag{2}$$

The term containing the spin-orbit interaction, H_{SO}, is of the Rashba type, of the form

$$H_{\mathrm{SO}} = \frac{i\kappa}{2} \int d^2r \Psi^\dagger [(\boldsymbol{\sigma} \times \boldsymbol{\nabla}) \cdot \hat{\boldsymbol{z}}] \Psi + \mathrm{H.c.} \tag{3}$$

We may write the SOC in component form,

$$H_{\mathrm{SO}} = \frac{\kappa}{2} \int d^2r [\psi_2^* \partial_x \psi_1 - \psi_1^* \partial_x \psi_2 + i\psi_2^* \partial_y \psi_1 + i\psi_1^* \partial_y \psi_2] + \mathrm{H.c.} \tag{4}$$

To simplify the representation of the potential term, we introduce the following parametrization: $\alpha_1 = \alpha(1-\Delta), \alpha_2 = \alpha(1+\Delta)$, $g_{11} = g(1-\gamma)$, $g_{22} = g(1+\gamma)$, and $g_{12} = \lambda g$. Δ thus tunes the imbalance of the components, γ tunes the relative strengths of the intracomponent density-density interactions, while λ tunes the strength of the intercomponent density-density interaction. The latter is responsible for producing a phase-separated state.

This particular Ginzburg-Landau theory has been much studied in the literature in the absence of SOC. It features a rich phase diagram where either one or both of the condensates may exist. In three dimensions, the phases are separated by first- or second-order phase transitions, depending on the details of the model [34]. The main impact of SOC is to produce a qualitatively new feature compared to the case without SOC, namely a nonuniform ground state; see below.

B. Lattice formulation

To arrive at a lattice model suitable for Monte Carlo simulations, we discretize the continuous fields ψ_i on a square grid, that is, we let $\psi_i \to \psi_{\boldsymbol{r},i}$, where $\boldsymbol{r} = (r_x, r_y)$, $r_\mu \in (1, \ldots, L)$, and $\mu \in (x, y)$. The derivatives are converted to forward finite differences through the replacement

$$\partial_\mu \psi_i \to \frac{1}{a} (\psi_{\boldsymbol{r}+\hat{\boldsymbol{\mu}},i} - \psi_{\boldsymbol{r},i}), \tag{5}$$

where $\hat{\boldsymbol{\mu}}$ is a unit vector in the μ direction, and a is the lattice spacing. We suppress the lattice spacing in the following expressions, real-space distances are plotted in units of a, while reciprocal space is plotted in units of $2\pi/La$. By introducing

real amplitudes and phases, $\psi_{\boldsymbol{r},i} = |\psi_{\boldsymbol{r},i}| \exp(i\theta_{\boldsymbol{r},i})$, we may write the derivatives of the Hamiltonian in terms of trigonometric functions.

We write the Hamiltonian as a sum of three terms as follows:

$$H = H_K + H_{\rm SO} + H_V. \tag{6}$$

H_K contains the kinetic terms, which are written in the standard cosine formulation

$$H_K = \sum_{\mathbf{r},\hat{\boldsymbol{\mu}},i} (|\psi_{\mathbf{r}}|^2 - |\psi_{\mathbf{r}+\hat{\boldsymbol{\mu}},i}||\psi_{\mathbf{r},i}| \cos \Delta_\mu \theta_{\mathbf{r},i}). \tag{7}$$

The potential term, with the new parametrization, is now written as

$$\begin{aligned} H_V = \sum_{\mathbf{r}} [&-\alpha(1-\Delta)|\psi_{\boldsymbol{r},1}|^2 - \alpha(1+\Delta)|\psi_{\boldsymbol{r},2}|^2 \\ &+ g(1-\gamma)|\psi_{\boldsymbol{r},1}|^4 + g(1+\gamma)|\psi_{\boldsymbol{r},2}|^4 \\ &+ 2g\lambda|\psi_{\boldsymbol{r},1}|^2|\psi_{\boldsymbol{r},2}|^2]. \end{aligned} \tag{8}$$

The SOC term on the lattice may also be described in terms of trigonometric functions. By replacing the differential operators of Eq. (4) by the forward difference representation of Eq. (5), and then replacing the complex fields with the amplitude and phase representation, we may write this particular term of the Hamiltonian as

$$\begin{aligned} H_{\rm SO} = -\kappa \sum_{\mathbf{r}} [&|\psi_{\boldsymbol{r},1}||\psi_{\boldsymbol{r}+\hat{\boldsymbol{x}},2}| \cos(\theta_{\boldsymbol{r}+\hat{\boldsymbol{x}},2} - \theta_{\boldsymbol{r},1}) \\ &- |\psi_{\boldsymbol{r},2}||\psi_{\boldsymbol{r}+\hat{\boldsymbol{x}},1}| \cos(\theta_{\boldsymbol{r}+\hat{\boldsymbol{x}},1} - \theta_{\boldsymbol{r},2}) \\ &+ |\psi_{\boldsymbol{r},1}||\psi_{\boldsymbol{r}+\hat{\boldsymbol{y}},2}| \sin(\theta_{\boldsymbol{r}+\hat{\boldsymbol{y}},2} - \theta_{\boldsymbol{r},1}) \\ &+ |\psi_{\boldsymbol{r},2}||\psi_{\boldsymbol{r}+\hat{\boldsymbol{y}},1}| \sin(\theta_{\boldsymbol{r}+\hat{\boldsymbol{y}},1} - \theta_{\boldsymbol{r},2})]. \end{aligned} \tag{9}$$

C. London model

Thermal fluctuations of the phases of the complex order parameter component are the most relevant fluctuations. Hence, it is useful first to neglect the amplitude fluctuations and consider a London model of the problem. Toward that end, we write the complex fields as $\psi_i = \rho_i \exp i\theta_i$, where only the phase θ_i is allowed to fluctuate. Note that this also implies that we assume the amplitudes to be uniform. To arrive at a London formulation, we write the Ginzburg-Landau Hamiltonian of Eq. (1) in component form, and we replace the complex fields with a constant amplitude and a fluctuating phase, as described above. This gives

$$\begin{aligned} H = \int d^2r \Bigg[&\sum_i \frac{\rho_i^2}{2} (\nabla\theta_i)^2 \\ &- \kappa\rho_1\rho_2[\sin(\theta_1 - \theta_2)\partial_x(\theta_1 + \theta_2) \\ &+ \cos(\theta_1 - \theta_2)\partial_y(\theta_1 + \theta_2)] \Bigg], \end{aligned} \tag{10}$$

such that two composite variables with very different behaviors emerge. On the one hand, $\theta_- \equiv \theta_1 - \theta_2$ has a preferential value: in the presence of the gradients of the phase sum, the second term in the above equations has phase-locking effects. On the other hand, $\theta_+ \equiv \theta_1 + \theta_2$ has first-order gradient terms, which may make it energetically favorable to modulate this phase. As the SOC term couples the two variables, there may be a subtle interplay between them influencing the phase transitions of the model.

The scaling dimension of the SOC term will be one less than that of a Josephson coupling (a Josephson term has no derivatives, while the SOS term has a single derivative). The SOC coupling is therefore less relevant, in a renormalization-group sense, than the Josephson coupling. A Josephson coupling is a singular perturbation on the system where Josephson coupling is absent, being highly relevant at any strength of the coupling [see, for instance, Appendix E of Ref. [35], in particular the discussion following Eq. (E7)]. It leads to a locking of phases of the complex order parameters of each component of the condensate, thus reducing the symmetry of the system from $U(1)\times U(1)$ to $U(1)$ (for the two-component case we study in this paper). On the other hand, the scaling dimension of the SOC term is one higher than current-current interactions in a multicomponent BEC, a so-called Andreev-Bashkin term [36,37], which leaves the $U(1)\times U(1)$ symmetry of the uncoupled system intact. The SOC coupling is an interesting case falling in between these two cases. Namely, at a given imbalance, a critical value of the SOC must be reached before the SOC term leads to a nonuniform ground state. Below this critical strength, the system effectively is represented (ignoring for the moment many-body interactions) as two independent condensates with $U(1)\times U(1)$ symmetry. Above the critical value of SOC, the system takes up a finite-momentum ground state. The SOC then effectively acts as a finite-momentum phase-locking Josephson coupling, as we shall see below.

Below, we will perform a mean-field analysis, where we assume that the phases and amplitudes of the boson condensate are modulated by some wave vector, which is included as a variational parameter when the free energy is minimized. This result may be compared to the previous work done on SOC bosons. We also compare the mean-field analysis to Monte Carlo simulations of the interacting lattice model.

D. Observables

The phase transition observed at $\kappa = 0$ is classified by examining the helicity modulus, defined by

$$\langle \Upsilon_{i,\mu} \rangle \equiv \frac{1}{V} \frac{\partial^2 F(\Delta_{i,\mu})}{\partial \Delta_{i,\mu}^2}, \tag{11}$$

along with the fourth-order modulus

$$\langle \Upsilon_{4,i,\mu} \rangle \equiv \frac{1}{V^2} \frac{\partial^4 F(\Delta_{i,\mu})}{\partial \Delta_{i,\mu}^4}, \tag{12}$$

where $\Delta_{i,\mu}$ is an infinitesimal twist applied to the phase $\theta_{r,i}$ in the μ direction, and $F(\Delta_{i,\mu})$ is the free energy with this twist applied. The transition manifests itself as a discontinuity in the helicity modulus in the thermodynamic limit. This translates to a dip in the fourth-order modulus that does not vanish in the thermodynamic limit. See Appendix for more details. As the x and y directions are equivalent, we will consider the average of $\Upsilon_{i,x}$ and $\Upsilon_{i,y}$ denoted by $\Upsilon_{i,\perp}$, as well as the average of $\Upsilon_{4,i,x}$ and $\Upsilon_{4,i,y}$ denoted by $\Upsilon_{4,i,\perp}$.

To examine the thermal melting of the spin-orbit-induced ground-state modulation, we calculate the specific heat, C_v. It

is given as fluctuations of the Hamiltonian,

$$C_V = \beta^2(\langle H^2\rangle - \langle H\rangle^2). \tag{13}$$

To compare the Monte Carlo results to mean-field calculations, we measure the average amplitude u_i, defined as

$$u_i = \left\langle \sum_{\boldsymbol{r}} |\psi_{i,r}|^2 \right\rangle. \tag{14}$$

Note that we use the same notation for both the mean-field value and the thermal average of $|\psi_i|^2$. It should be clear from the context which one is discussed. We also measure the thermal average of the density as a function of position, $\langle|\psi_i(\boldsymbol{r})|^2\rangle$, to examine possible modulations in the density substrate. To monitor the thermal fluctuations in the condensate densities, we compute their probability distribution, $\mathcal{P}(|\psi_i|^2)$, by making a histogram of the field configurations at each measuring step of the Monte Carlo simulations.

To monitor the formation of the modulated ground state, we compute the phase correlation function, defined by

$$G_X(\boldsymbol{r},\boldsymbol{r}') = \langle e^{i\theta_{r,X}} e^{-i\theta_{r',X}}\rangle. \tag{15}$$

Here, X may represent either component 1 or 2, as well as the sum or difference of the two, $\theta_1+\theta_2$ and $\theta_1-\theta_2$. We also calculate its Fourier transform, the phase structure function, defined by

$$G_X(\boldsymbol{q}) = \frac{1}{V}\sum_{\boldsymbol{r},\boldsymbol{r}'} e^{i\boldsymbol{q}\cdot(\boldsymbol{r}-\boldsymbol{r}')} G_X(\boldsymbol{r},\boldsymbol{r}'). \tag{16}$$

At large distances, r, the correlation function is expected to scale as $G_X(r)\sim r^{-\eta}$. We measure this exponent by extracting the value of $G_X(\boldsymbol{q})$ at a particular value, $\boldsymbol{Q}$, which in turn defines the exponent $\eta_{\boldsymbol{Q}}$ as

$$G_X(\boldsymbol{Q}) \sim L^{2-\eta}. \tag{17}$$

III. MEAN-FIELD THEORY

Intercomponent density interactions suppress the minority condensate at sufficiently strong values of the coupling value. To get crude estimates for the interaction parameters needed for this to occur, we start out by considering the model in the mean-field approximation. The full fluctuation spectrum of the bosonic ordering fields will be considered in subsequent sections. Here, we give the mean-field theory in a continuum model.

To account for the fact that the ground state is generically modulated in the presence of SOC, we assume that the complex fields ψ_i are given in terms of a mean-field value plus fluctuations, multiplied by a spatial plane-wave modulation with momentum $\boldsymbol{q}$. In general, we may use the ansatz [38,39]

$$\psi_{1,\boldsymbol{q}} = \sqrt{u_1+\delta u_1}\exp i(\phi_1+\delta\phi_1-\arg\boldsymbol{q}+\boldsymbol{q}\cdot\boldsymbol{r}), \tag{18}$$

$$\psi_{2,\boldsymbol{q}} = \sqrt{u_2+\delta u_2}\exp i(\phi_2+\delta\phi_2+\boldsymbol{q}\cdot\boldsymbol{r}), \tag{19}$$

where $\arg\boldsymbol{q}$ is the orientation of $\boldsymbol{q}$ with respect to some reference axis. Specifically, we follow previous work [38,39] and assume that the ground state is either modulated by a single wave vector (denoted Ψ_0) or by two oppositely aligned wave vectors (denoted Ψ_π). That is,

$$\Psi_0 = \begin{pmatrix}\psi_{1,\boldsymbol{q}}\\ \psi_{2,\boldsymbol{q}}\end{pmatrix} \tag{20}$$

and

$$\Psi_\pi = \frac{1}{2}\begin{pmatrix}\psi_{1,\boldsymbol{q}}+\psi_{1,-\boldsymbol{q}}\\ \psi_{2,\boldsymbol{q}}+\psi_{2,-\boldsymbol{q}}\end{pmatrix} = \begin{pmatrix}-\sqrt{u_1+\delta u_1}e^{i\phi_1+i\delta\phi_1-i\bar\theta}\sin\boldsymbol{q}\cdot\boldsymbol{r}\\ \sqrt{u_2+\delta u_2}e^{i\phi_2+i\delta\phi_2}\cos\boldsymbol{q}\cdot\boldsymbol{r}\end{pmatrix}, \tag{21}$$

where $\bar\theta$ is the average angle of $\boldsymbol{q}$ and $-\boldsymbol{q}$ with respect to the x axis. Here, the amplitudes, phases, and wave vectors are to be regarded as variational parameters in the mean-field free energy of the modulated state.

Inserting these expression into Eq. (1) and using the mean-field values only, we obtain the two free-energy densities f_0 and f_π,

$$f_0 = \frac{|\boldsymbol{q}|^2}{2}(u_1+u_2) - 2|\boldsymbol{q}|\kappa\sqrt{u_1u_2}\sin(\phi_1-\phi_2)+V_0. \tag{22}$$

$$f_\pi = \frac{|\boldsymbol{q}|^2}{4}(u_1+u_2) - |\boldsymbol{q}|\kappa\sqrt{u_1u_2}\cos(\phi_1-\phi_2)+V_\pi. \tag{23}$$

Here, the potentials V_0 and V_π differ slightly due to numerical factors obtained when integrating over space. They have the forms

$$V_0 = -\alpha[(1-\Delta)u_1+(1+\Delta)u_2] + g\left[(1-\gamma)u_1^2+(1+\gamma)u_2^2+2\lambda u_1u_2\right] \tag{24}$$

and

$$V_\pi = -\frac{\alpha}{2}((1-\Delta)+u_1(1+\Delta)u_2) + \frac{g}{8}\left[3(1-\gamma)u_1^2+3(1+\gamma)u_2^2+2\lambda u_1u_2\right]. \tag{25}$$

Note from Eqs. (22) and (23) that in a modulated ground state, the SOC essentially acts as a phase locking on $\phi_1-\phi_2$ in a system with a uniform ground state. We may minimize Eqs. (22) and (23) with respect to this phase difference, assuming that $|q|\neq 0$ and $u_i\neq 0\ \forall\ i$, which yields a phase locking of $\phi_1-\phi_2=\pi/2$ for f_0 and $\phi_1-\phi_2=0$ for f_π. The angle $\arg\boldsymbol{q}$ in the single q-vector case and the average angle $\bar\theta$ drop out of the equations, which reflects the degeneracy of the single-particle spectrum.

Considering the modulation vector present in Eqs. (22) and (23) as a variational parameter, and assuming $u_i\neq 0\ \forall\ i$, we find

$$|\boldsymbol{q}| = \frac{2\kappa\sqrt{u_1u_2}}{u_1+u_2} \tag{26}$$

in both cases. With this solution inserted into the free-energy densities, they become

$$f_0 = -\frac{2\kappa^2u_1u_2}{u_1+u_2}+V_0 \tag{27}$$

and

$$f_\pi = -\frac{\kappa^2u_1u_2}{u_1+u_2}+V_\pi. \tag{28}$$

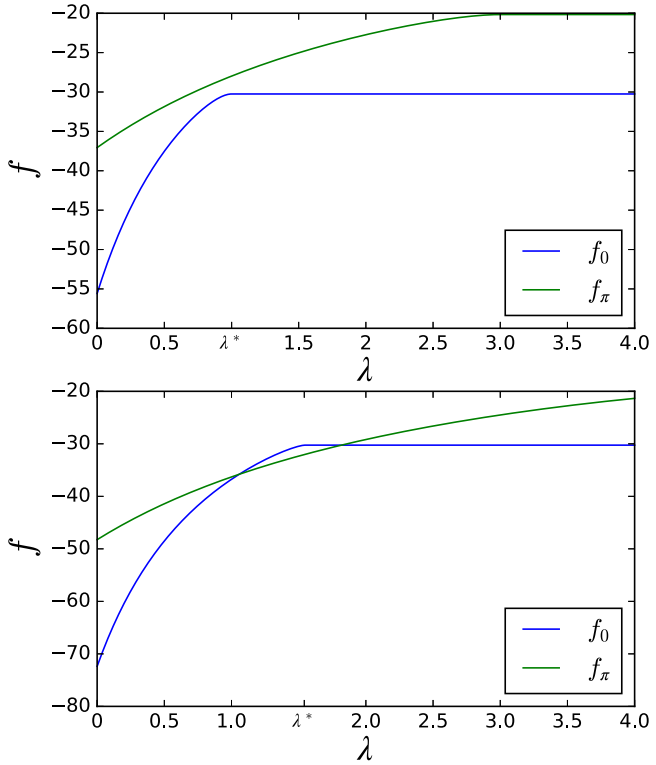

FIG. 1. Results for minimum values of f_0 and f_π as a function of λ for two values of κ. Top panel: $\kappa = 1$. Bottom panel: $\kappa = 2$. Note how f_0 ceases to be dependent on λ for large λ, at some value λ^*. Note also the discontinuity in the derivative of f_0 at $\lambda = \lambda^*$.

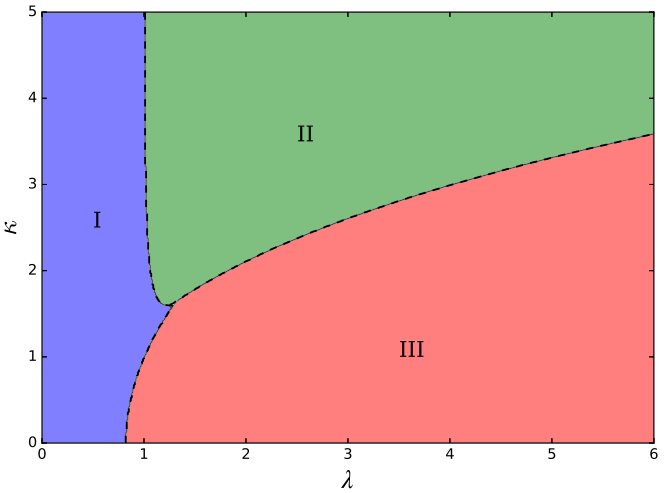

FIG. 2. Mean-field phase diagram in the λ-κ plane, with other parameters $\alpha = 10.0$, $g = 1.0$, $\Delta = 0.1$, $\gamma = 0.0$, and $m = 1.0$. Regions I and III are the regions where both components exist and the effect of SOC is present, resulting in a ground state at finite momentum. In region I, the ground state is modulated by a single wave vector. In region III, the ground state is modulated by two oppositely directed wave vectors. Region II is the region where the intercomponent interactions suppress the minority condensate, which results in a single-component condensate at zero momentum.

Equations (27) and (28) may be solved, in principle, for u_1 and u_2, but as they are cubic, the expressions for the solutions are unwieldy and not particularly illuminating. Instead, we numerically minimize both free-energy densities, and then we determine the ground state for a given parameter range by finding $\min(f_0, f_\pi)$. This gives the regions of the phase diagram where the ground state is modulated by either one or two wave vectors. For the SOC to be effective, it is also required that $u_1 u_2 \neq 0$. For $u_1 u_2 = 0$, the model reverts to a single-component condensate, i.e., a "spinless" model where SOC cannot be operative.

In Fig. 1, we plot a few representative values of f_0 and f_π as a function of λ for two values of κ. For the lowest value of κ, it is seen that $f_0 < f_\pi$ for all values of λ. Hence, a ground state modulated by two q-vectors is not found. For a larger value of κ, $f_0 < f_\pi$ for low and high values of λ, while for intermediate values of λ, $f_\pi < f_0$. Thus, for large enough κ and intermediate values of λ, there is the possibility of finding ground states modulated by two q-vectors.

Moreover, it is seen that for both values of κ, f_0 is independent of λ when λ reaches some value $\lambda = \lambda^*$. This happens at the value for which the minority condensate (u_1 in this case) is completely suppressed. Furthermore, the second crossing of f_0 and f_π always occurs at values of $\lambda > \lambda^*$. Therefore, for given κ and with increasing λ, the ground state modulated by two q-vectors always transitions into a uniform ground state with one condensate completely suppressed.

Note also that f_0 increases more rapidly with λ than f_π. This is due to the difference in the potentials V_0 and V_π, Eqs. (24) and (25). Therefore, having two crossings of f_0 and f_π as a function of λ means that one of the crossing points must always be to the right of the point where f_0 becomes λ-independent. Thus, f_0 being minimal always transitions into f_π being minimal II as λ increases. There will never be a transition from f_π being minimal back to f_0 being minimal with increasing λ.

This may be summarized as follows. In Fig. 2, we show the results of numerically solving Eqs. (27) and (28) in the λ-κ plane. Region I represents the area where the single-q modulated ground state is preferred, region III where the two-q modulated ground state is preferred, and region II is the area where $u_1 u_2 = 0$ minimizes the free energy, making this state a uniform, single-component state. The two lines separating I and II, and II and III, are located by the crossings of the free energies f_0 and f_π, and they therefore represent first-order phase transitions at the mean-field level. The line separating regions I and II is a direct transition between a ground state modulated by one q-vector and a uniform ground state, without an intermediate ground state modulated by two q-vectors. The location of this line is therefore determined by the value of λ where f_0 ceases to be dependent on λ, while f_π represents a higher-energy state that is irrelevant. The order of this phase transition is determined by whether $\partial f_0/\partial\lambda$ is continuous or discontinuous at λ_c. We have $\partial f_0/\partial\lambda \approx (\partial f_0/\partial u_1)(\partial u_1/\partial\lambda)$. Using Eq. (27), we see that this is determined by $\partial u_1/\partial\lambda$. Since u_1 vanishes in a finite interval in λ, $\partial u_1/\partial\lambda$ has to be discontinuous at λ^*, and hence so does f_0. The transition line separating I and II is therefore also first-order.

IV. DETAILS OF THE MONTE CARLO SIMULATIONS

The model is simulated using the Monte Carlo algorithm with a simple restricted update scheme of each physical variable, using Metropolis-Hastings [40,41] tests for acceptance. The model is discretized on a rectangular lattice of size $L_x \times L_y$, with periodic boundary conditions. Typically, 5×10^6 Monte Carlo sweeps are used at each temperature step, with an additional 5×10^5 sweeps discarded for equilibration. One sweep consists of attempting to update each physical variable on each lattice site once in succession. The proposed new value for each variable is picked within a restricted region around the old value, where the size of the region is chosen to allow for both high acceptance rates and low autocorrelation times. To further minimize autocorrelation times and increase simulation efficiency, we measure observables with a period of 100 Monte Carlo sweeps. Pseudorandom numbers are generated with the Mersenne-Twister algorithm [42]. During equilibration, time series of the internal energy is examined for convergence, this ensures proper equilibration. To avoid metastable states, several simulations with identical parameters but differing initial seeds of the pseudorandom number generator are performed to make sure they anneal to the same state. Measurements are postprocessed using multiple-histogram reweighting [43], and error estimates are determined with the jackknife method [44].

The allowed range of amplitude fluctuations is determined during the equilibration procedure by first allowing it to fluctuate to a very large value ($|\psi_i|^2 \sim 10$ was typically used) and then reducing the value to include all values that had a nonzero probability of being picked according to the measured probability distribution, $\mathcal{P}(|\psi_i|^2)$.

Unless otherwise stated, we set $\alpha_0 = 10.0$, $g = 1.0$, and $\gamma = 0.0$. The large value of $\alpha_0 = 10.0$ is chosen to have sharp probability distributions of the amplitudes. Generally, a square lattice of $L_x = L_y \equiv L = 64$ is used in simulations, but system sizes of $L \in (16,24,32,40,48,56,64,96, 128,160,192,224,256)$ are used for performing a finite-size-scaling (FSS) analysis.

V. RESULTS OF THE MONTE CARLO SIMULATIONS

In this section, we present Monte Carlo simulations to corroborate and expand on the arguments given in the previous sections. The model exhibits three different classes of BECs for different parameter regimes. For strong intercomponent interactions and zero to intermediate SOC, there will be only one superfluid condensate present. With no SOC, but for intermediate intercomponent interactions, the model is a two-component coupled superfluid. Finally, for intermediate interactions and SOC, the model is a two-component superfluid with a finite q-vector. This schematic picture shown in Fig. 2 is captured by a simple mean-field argument, but we find it to be essentially correct also when thermal fluctuations are taken into account in Monte Carlo simulations. We also examine the thermal phase transitions present in the cases of zero SOC and when the condensate is modulated by a single q-vector.

A. Kosterlitz-Thouless transition in the absence of spin-orbit coupling

When $\kappa = 0$, the model represents a two-component BEC coupled by density-density interactions, which may collapse to a single-component condensate for strong intercomponent interactions. When neglecting amplitude fluctuations (which of course decouples the condensates), the model reduces to the XY model. Here, the low-temperature phase is characterized by quasi-long-range order of the superfluid order parameter, where vortices and antivortices form bound pairs. As the temperature is increased, the bound vortex-antivortex pairs unbind at a Kosterlitz-Thouless (KT) transition [45,46]. As a check of simulations, we indeed obtain that the two-component model with amplitude fluctuations included belongs in the KT universality class by establishing that the helicity modulus undergoes a discontinuous jump to zero as the system is heated from the low-temperature state, with the value of the jump close to the predicted universal value. We examine various values for the intercomponent coupling λ, and we find that the above remains true for all the values of λ we have considered.

Figure 3 shows the helicity modulus and fourth-order modulus of component 2 for system sizes $L \in (16,24,32, 40,48,56,64)$ with intercomponent coupling strength $\lambda = 2.0$. The inset shows the depth of the dip in the fourth-order modulus as a function of inverse linear system size. By fitting the helicity modulus to Eq. (A8), we determine the discontinuous jump to be $\Upsilon(\infty)\beta_c = 0.650(1)$ at $\beta_c = 0.282$. Extrapolation of the value of the negative dip to $1/L = 0$ gives a finite value of 0.49(1). This is clear evidence for a discontinuous jump in the helicity modulus, placing the transition in the Kosterlitz-Thouless universality class.

Similar results are obtained for values of $\lambda \in (0.0,0.25,0.5, 0.75,1.25,1.5,1.75,2.0)$, as shown in Table I. For the values of λ where both condensates persist, transitions of KT type are observed in both components, at different critical couplings. In all cases considered, the value of the minimum in Υ_4 converges to a nonzero value. This demonstrates that there is a discontinuous jump in the helicity modulus, regardless of the value of the intercomponent interaction strength, and whether or not the minority condensate is depleted. Additionally, the value of the discontinuous jump varies weakly with λ, and is close to the universal value of $2/\pi$. This indicates that fluctuations in the condensate amplitude only have a minor effect on the details of the transition. None of the obtained jumps is within the prediction $2/\pi$, with error estimates, but most are close. Moreover, the fitting routine was sensitive to the system sizes that were included. Both effects may have been caused by the inclusion of amplitude fluctuations. Also note that the critical temperature and depth of the dip varies very weakly with λ, as long as $\lambda \geqslant 1.0$. This is very reasonable, as the model is effectively a single-component condensate in this regime, so varying the intercomponent interaction strength should have little to no effect.

Finally, we remark that the fit of the discontinuous jump and the determination of the depth of the dip in the fourth-order modulus are two independent methods for detecting a KT transition. As both methods give good results consistent with the KT prediction, we are confident in claiming that the two-component imbalanced BEC without SOC has one or

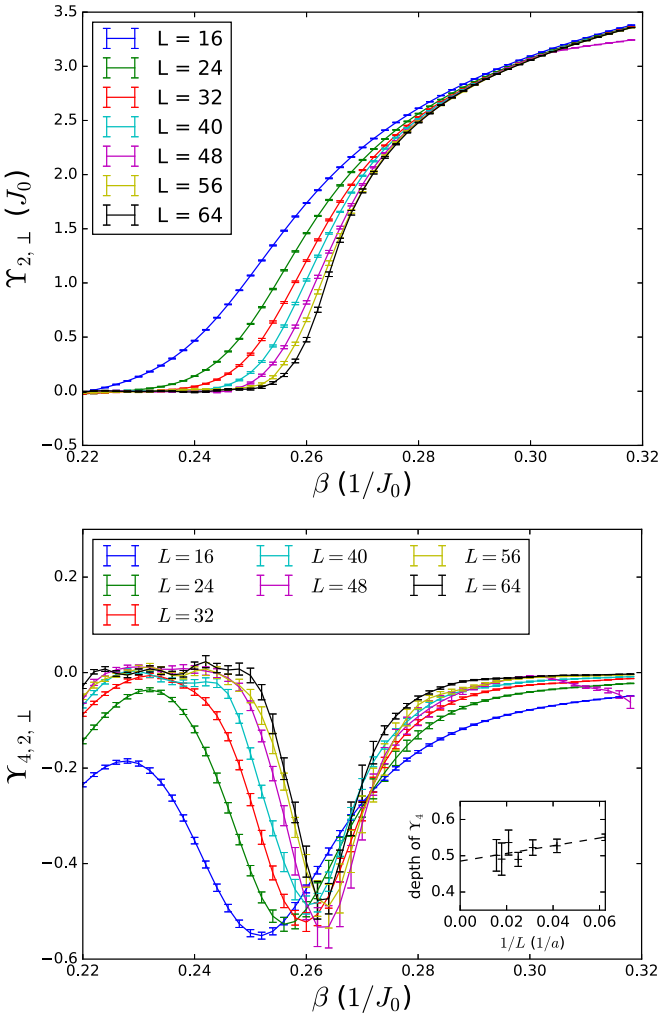

FIG. 3. Helicity modulus (top panel) and fourth-order modulus (bottom panel) of component 2 as a function of β for several system sizes, with $\lambda = 2.0$ and $\kappa = 0.0$. The inset of the bottom figure shows the value of the dip in the fourth-order modulus as a function of inverse system size. The dashed line is a linear extrapolation to the thermodynamic limit. At this value of the intercomponent coupling strength, the condensate density of component 1 is extinguished, and hence it exhibits no KT transition.

two transitions, depending on the value of the intercomponent coupling strength, in the KT universality class. However, pinning down a KT transition with great confidence is notoriously difficult. In particular, Eq. (A8) involves slowly decaying corrections that are suppressed only logarithmically. Several works [47,48] have successfully utilized this particular method in various models, and methods to overcome the slowly decaying corrections do exist [49]. A detailed study of this is not the main focus of the present paper. We limit ourselves to noting that our results are consistent with a KT transition, as is expected for the model in the absence of SOC.

B. Spin-orbit induced modulated ground states

Preliminary arguments based on the noninteracting energy spectrum and mean-field calculations suggest that the ground state of the spin-orbit coupled BEC resides at either one or two finite q-vectors. To confirm this, Monte Carlo simulations of the full lattice model, Eqs. (6)–(9), were performed in parameter regions corresponding to regions I and III in the phase diagram of Fig. 2.

1. Single q-vector

To observe the predicted modulated state in which a single q-vector is present, we perform simulations of the lattice model at $\kappa = 1.0$ and $\lambda = 0.0$. Figure 4 shows the real parts of the phase-correlation function, Eq. (15), and the structure factors of the phase-sum and phase-difference variable in the low-temperature phase, when the inverse temperature is $\beta = 1.5$. The phase-correlation function Eq. (15) for the phase-sum composite variable is modulated with a single q-vector along the diagonal. The phase-difference composite variable shows no modulation. It is, however, highly correlated, which is a result of the effective Josephson locking. This is in accord with expectations based on the London approximation, where amplitudes are frozen; see Eq. (10). The London case, with nonmodulated amplitudes, suffices to describe the situation with relatively small values of intercomponent density-density interactions, where amplitudes are constant throughout the system. The SOC term tends to lock $\theta_1 - \theta_2$ at constant value, since the strength of the SOC term is effectively constant due to the constant values of the amplitudes, while SOC induces

TABLE I. Summary of the results obtained when searching for the KT transition. Each row shows, for both components, the critical inverse temperature with the best fit to Eq. (A8), β_c, the size of the jump at this inverse temperature, $\Upsilon_\infty\beta_c$, as well as the extrapolation of the value of the minimum in the fourth-order modulus to $1/L = 0$. When $\lambda \geqslant 1.0$, the density of component 1 has been completely depleted, and there is no phase transition in this sector, as signified by the entries marked N/A.

	Component 1			Component 2		
λ	β_c	$\Upsilon_\infty\beta_c$	Value of minimum in Υ_4	β_c	$\Upsilon_\infty\beta_c$	Value of minimum in Υ_4
0.00	0.280	0.617(1)	0.56(3)	0.226	0.642(2)	0.58(7)
0.25	0.391	0.609(1)	0.367(8)	0.249	0.5(3)	0.67(3)
0.50	0.605	0.595(1)	0.239(9)	0.284	0.625(1)	0.49(3)
0.75	2.24	0.58(1)	0.068(4)	0.290	0.627(1)	0.50(2)
1.00	N/A	N/A	N/A	0.292	0.662(1)	0.48(2)
1.25	N/A	N/A	N/A	0.290	0.667(1)	0.46(3)
1.50	N/A	N/A	N/A	0.290	0.703(1)	0.50(1)
1.75	N/A	N/A	N/A	0.284	0.653(1)	0.61(5)
2.00	N/A	N/A	N/A	0.282	0.650(1)	0.49(1)

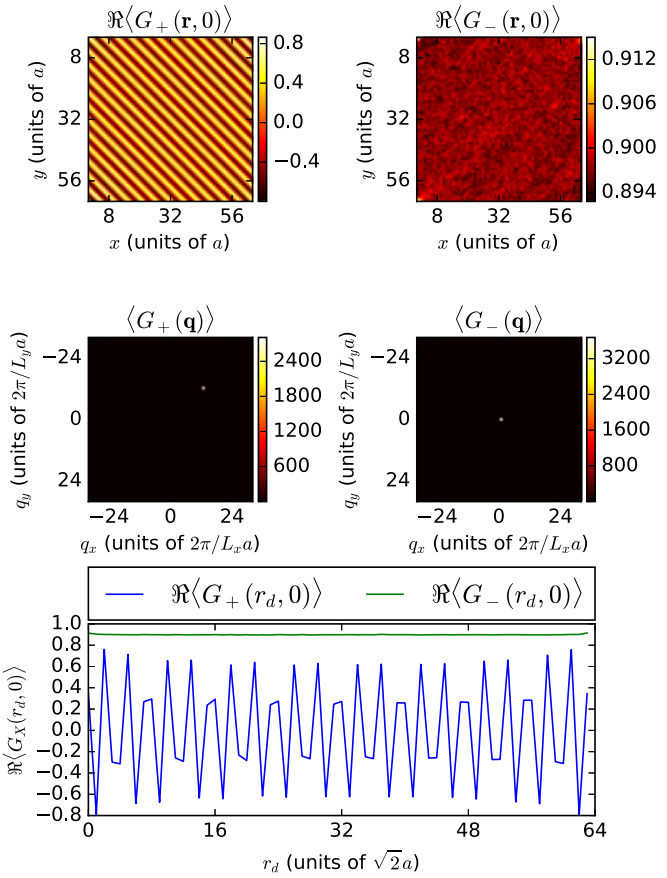

FIG. 4. The real part of the phase correlation function Eq. (15) in real (top row) and reciprocal (middle row) space of the phase sum (left column) and phase difference (right column), at parameters $\kappa = 1.0$, $\lambda = 0.0$, and $\beta = 1.0$. The bottom panel shows a real-space cut along the diagonal perpendicular to the stripes, r_d, of both the phase-sum and phase-difference correlation functions. The effect of the SOC is manifest in the phase sum, which is modulated by a wave vector, $\boldsymbol{Q}$. The phase difference exhibits no modulations in the spatial correlation. We have removed the reference point $\boldsymbol{r} = \mathbf{0}$ from the real-space plots to improve the visibility of the correlations.

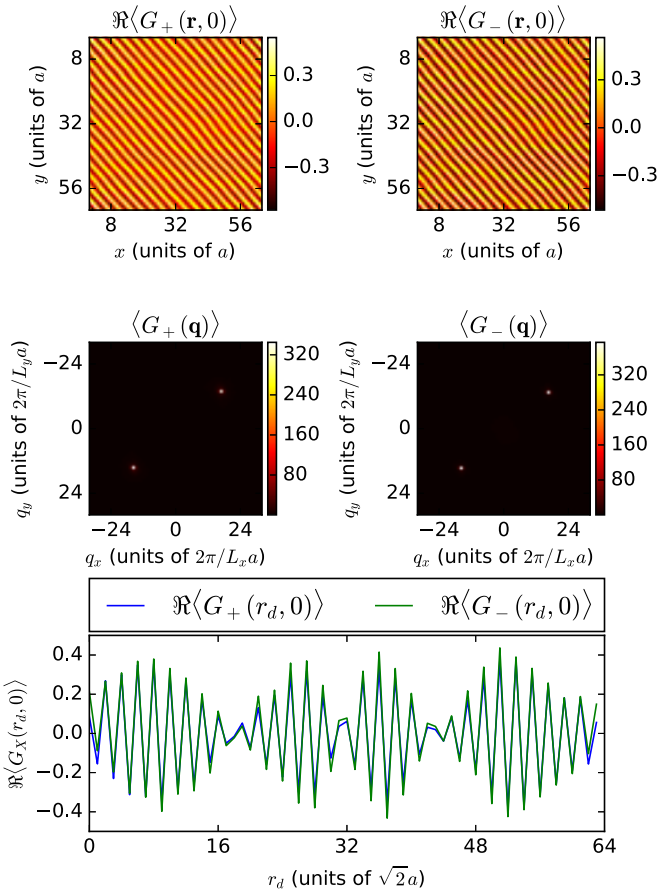

FIG. 6. Real part of phase-correlation function Eq. (15) in real (top row) and reciprocal (middle row) space of the phase sum (left column) and phase difference (right column), at parameters $\beta = 1.0$, $\lambda = 1.2$, and $\kappa = 1.7$. In the bottom panel, we also show a real-space cut along the diagonal perpendicular to the stripes, r_d, of both correlation functions. It is shown that both the phase sum and the phase difference are modulated by two oppositely aligned wave vectors, $\pm\boldsymbol{Q}$, with equal magnitude. We have removed the reference point $\boldsymbol{r} = \mathbf{0}$ from the real-space plots to improve the visibility of the correlations.

a gradient in $\theta_1 + \theta_2$. The $\theta_1 + \theta_2$ modulations, therefore, originate with SOC coupling.

In these simulations, the amplitudes are also allowed to fluctuate. The real-space amplitude plots shown in Fig. 5 show

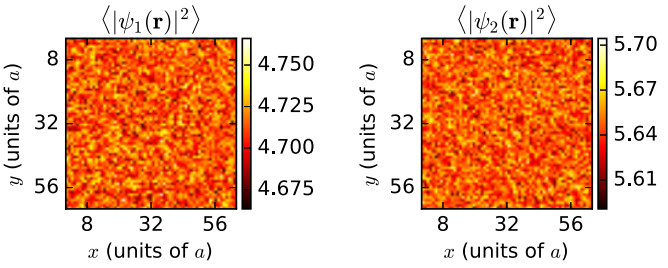

FIG. 5. Thermal amplitude averages in real space for component 1 (left panel) and 2 (right panel), at parameters $\kappa = 1.0$, $\lambda = 0.0$, and $\beta = 1.0$. There are only minor spatial fluctuations around the average, u_i, in each individual component.

that the spatial amplitude fluctuations are small. In this regime, the potential does not favor large density differences between the two components, and there is no phase separation. The state we observe is the same as was found in Refs. [25,27], where a single minimum in the noninteracting spectrum is populated for $\lambda < 1$.

2. *Double q-vector*

The ground state modulated by two oppositely directed q-vectors only occurs, in mean field, at sufficiently high values of both κ and λ. To observe this state, we perform simulations at $\kappa = 1.7$ and $\lambda = 1.2$, with $\beta = 1.0$, inside region III of Fig. 2. In Fig. 6, we show Monte Carlo calculations of the correlation function of the phase sum and difference in both real and reciprocal space. As in the single-q vector case, the phase-sum correlation is modulated, although now with a larger $|\boldsymbol{q}|$. The increase of the length of the q-vector directly reflects the larger value of the SOC strength.

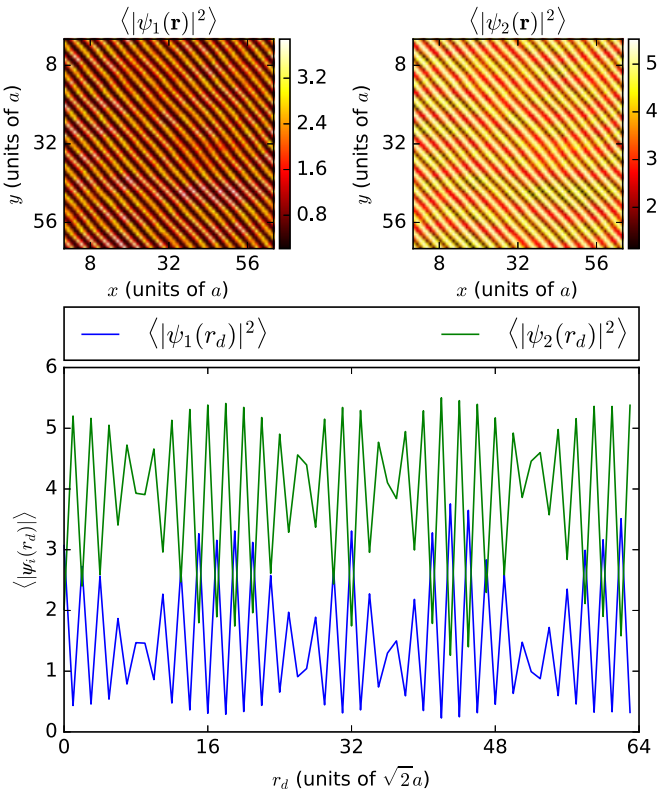

FIG. 7. Thermal amplitude averages in real space for components 1 (top row, left panel) and 2 (top row, right panel) at parameters $\beta = 1.0$, $\lambda = 1.2$, and $\kappa = 1.7$. The bottom panel shows a cut of the amplitude averages along the diagonal perpendicular to the stripe modulations, r_d. Both amplitudes are modulated in this region of parameter space, but around different mean values because of the density imbalance. Furthermore, the amplitude of component 1 is staggered compared to component 2. This minimizes the potential energy from the intercomponent density-density interaction while still minimizing the SOC interaction energy.

Another important difference between the double-q vector state compared to the single-q vector state is shown in Fig. 7, which shows the thermal averages of the amplitudes. In this case, the amplitudes are also modulated. Furthermore, the amplitudes of the two components are staggered when component 1 has a large amplitude, component 2 has a low amplitude, and vice versa. This is further exemplified in the bottom panel of Fig. 7, where we show a cut along the diagonal perpendicular to the stripes in the amplitude densities. Here it is clearly seen that the two amplitude variations are mirror images of each other, only shifted relative to each other by the difference in the average amplitudes due to the component imbalance.

Unlike the single-q vector case, the phase-difference correlation is also modulated. This may now be understood as follows. The system is in a parameter regime where λ is large enough to induce staggering of the amplitudes of the condensates in order to minimize energy. The London approximation, Eq. (10), therefore no longer suffices to describe the system, and we revert to Eq. (9). It is the term with the minus sign in H_{SO} that leads to the frustration of $\theta_1 - \theta_1$. Were this sign to be reversed, we would have had $\theta_1 - \theta_2 = 0$.

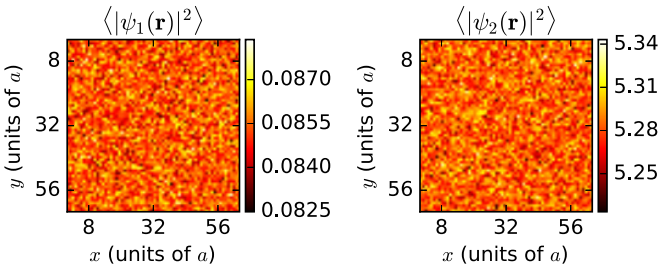

FIG. 8. Thermal amplitude averages in real space for components 1 (top row, left panel) and 2 (top row, right panel) at parameters $\kappa = 1.0$, $\lambda = 2.0$, and $\beta = 1.0$.

Since the amplitudes are modulated, so are the gradients of the amplitudes, and so is therefore the strength of the frustration in the phase difference. This difference is therefore itself modulated. The modulation of $\theta_1 - \theta_1$ therefore originates with the modulation of amplitudes, which is a consequence of strong intercomponent density-density interactions. Recall from above that the modulation of $\theta_1 + \theta_1$ originates with SOC.

C. Interaction-induced destruction of modulated ground states

The mean-field calculations presented in Sec. III predict a breakdown of the modulated ground state shown in Fig. 4 when the intercomponent interaction parameter, λ, reaches the threshold shown in Fig. 2, provided $\kappa \lesssim 1.5$. Above this threshold, the condensate transitions from a single-q condensate into a condensate modulated by two opposite wave vectors. For $\gamma = 0$ and $\Delta > 0$, which we consider here, component 1 is the minority component that collapses. The mechanism for the collapse is that intercomponent interactions drive the minority component to zero to eliminate the interaction energy. When the model collapses to an effective one-component model, there will be no effects of the SOC, as the q-vectors of the modulation induced by it are proportional to $u_1 u_2$ at the mean-field level.

To show this suppression, we compute the thermal amplitude averages of both components in the low-temperature phase, shown in Fig. 8, when $\beta = 1.0$, $\kappa = 1.0$, and $\lambda = 2.0$. That is, every parameter is identical to what is shown in Figs. 4 and 5, except the intercomponent interaction is increased above the critical value given by the mean-field calculations. It is evident that both amplitudes are now again unmodulated, but the amplitude of component 1 has been almost completely depleted. Its small finite value is only a remnant of the thermal fluctuations included in the simulations.

To further explore the effect of the depletion, we compute the phase-correlation function Eq. (15) and its Fourier transform, Eqs. (15) and (16). Figure 9 shows the real parts of both the phase-correlation function Eq. (15) and the structure factor of both individual components. There are no modulations in the phase-correlation function Eq. (15), and both structure factors are isotropic. However, while the phase of component 1 is completely uncorrelated, the phase of component 2 is strongly correlated. The reasons for this are that (i) the condensate amplitude of component 1 has been completely depleted, leaving the phase of this component completely uncorrelated

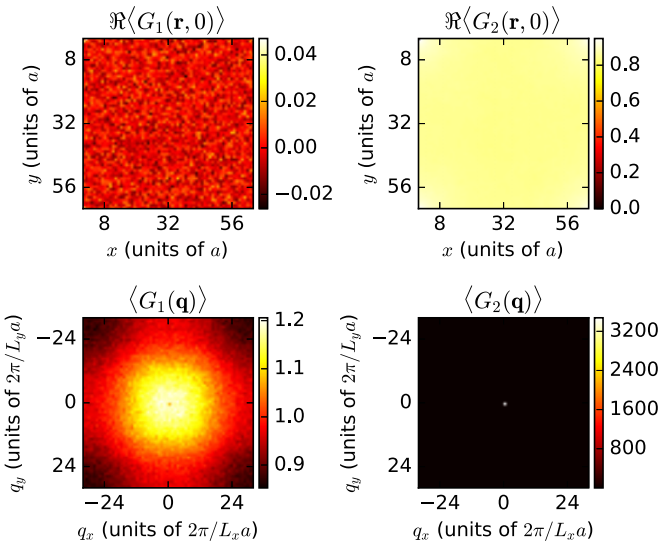

FIG. 9. Real part of the phase-correlation function Eq. (15) in real space (top row) and reciprocal space (bottom row) for the phase of component 1 (left column) and component 2 (right column) at parameters $\kappa = 1.0$, $\lambda = 2.0$, and $\beta = 1.0$. We have removed the reference point $\boldsymbol{r} = \mathbf{0}$ from the real-space plots to improve the visibility of the correlations.

at all temperatures, and (ii) the nonsuppressed condensate has entered a low-temperature superfluid state, akin to what we observe for $\kappa = 0$, even though we still have a finite SOC, however ineffective.

Figure 10 summarizes the results obtained in the Monte Carlo simulations, showing an overview of the different ground states obtained at slow annealing from a random initial state at high temperature down to $\beta = 6.0$, for different values

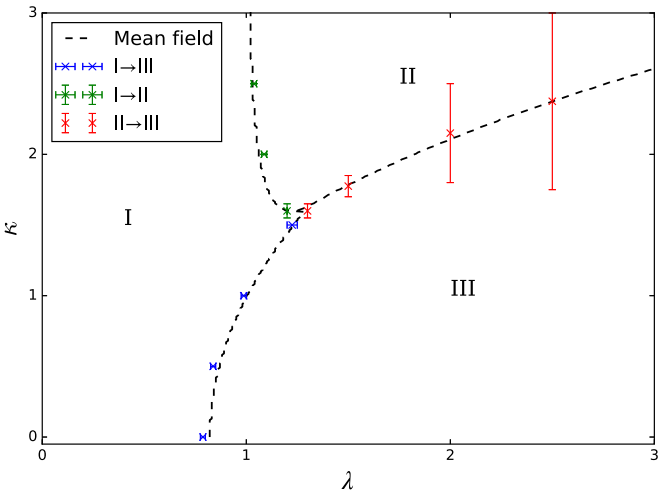

FIG. 10. Phase diagram obtained from numerical Monte-Carlo simulations compared to mean-field predictions. The points with error bars correspond to observed transition points, blue points correspond to the transition from region I to region II, green points correspond to the transition from region I to region III, and red points correspond to the transition from region II to region III. The dashed lines are the corresponding transition lines obtained from mean-field calculations shown in Fig. 2.

of (κ,λ). The size of region I was largely unaffected. For intermediate values of κ and sufficiently large values of λ, we observe that the spin-orbit-induced modulations of both the amplitudes and the phases are pinned to the crystal axes of the numerical lattice. This is represented by the large error bars of the red points denoting the transition from region II to region III obtained from the Monte Carlo simulations. We determine these particular error bars by finding the upper and lower limits in κ, where we can confidently observe a pure double q-vector condensate or a pure single-component condensate. That aside, the mean-field and MC calculations correspond remarkably well, even close to the area where the three transition lines meet.

D. Thermal disordering of single-q modulated state

The thermal fluctuations of the superfluid phases are also expected to disorder the modulated ground-state pattern induced by the SOC. The modulation that appears in region I at low temperatures is characterized by modulated superfluid order, or superfluid order with a texture. The temperature-driven disordering of this modulated superfluid state is expected to lie in the KT-universality class. To examine the thermal phase transition from the low-temperature phase of region I into the high-temperature phase, we perform simulations of the full Hamiltonian as written in Eq. (6) and in the London limit. The London limit is employed here as it is the minimal model that captures the effect of the SOC. As discussed in Sec. V B, in region I where the condensate is only modulated by a single $\boldsymbol{q}$-vector, we find that the amplitudes are essentially uniform. Hence, the amplitude fluctuations are largely irrelevant for this phase, and we may therefore employ the London limit. The London limit is taken by fixing $|\psi_{\boldsymbol{r},i}| = 1\ \forall\ \boldsymbol{r},i$, which simplifies the Hamiltonian greatly.

To determine the nature of the thermal phase transition that disorders the modulated superfluid, we measure the helicity modulus of the phase-sum variable, the exponent $\eta_{\boldsymbol{Q}}$, and the specific heat. The helicity modulus is modified compared to the case with no SOC, due to the extra terms in the Hamiltonian. The value of the exponent $\eta_{\boldsymbol{q}}$ is expected to approach the limit $1/4$ from below as the critical inverse temperature is approached from above [50]. In Figs. 11 and 12, we show the results of the simulations with and without amplitude fluctuations included, respectively. The top panels show the specific heat on the left axis, and the value of the exponent $\eta_{\boldsymbol{Q}}$ on the right axis. We also show the scaling of the specific-heat peak in the insets of the top panels, and we find its exponent to be 0.8(2) with amplitude fluctuations included, and 0.66(9) in the London limit. In the bottom panels, we show the helicity modulus of the phase-sum variable, both of which exhibit a sharp jump that coincides with the drop in the scaling exponent and the specific-heat peak. In both cases, the sharp peak of the specific heat with its large scaling exponent, the abrupt drop of the exponent $\eta_{\boldsymbol{Q}}$, and the sharp jump and large error bars of the helicity modulus all point toward a strong depinning transition separating the modulated superfluid phase and the normal fluid phase. A KT transition does not fit into the picture presented by Figs. 11 and 12, mainly because the specific heat at the KT-transition temperature has an essential singularity. This singularity is virtually undetectable in numerical simulations.

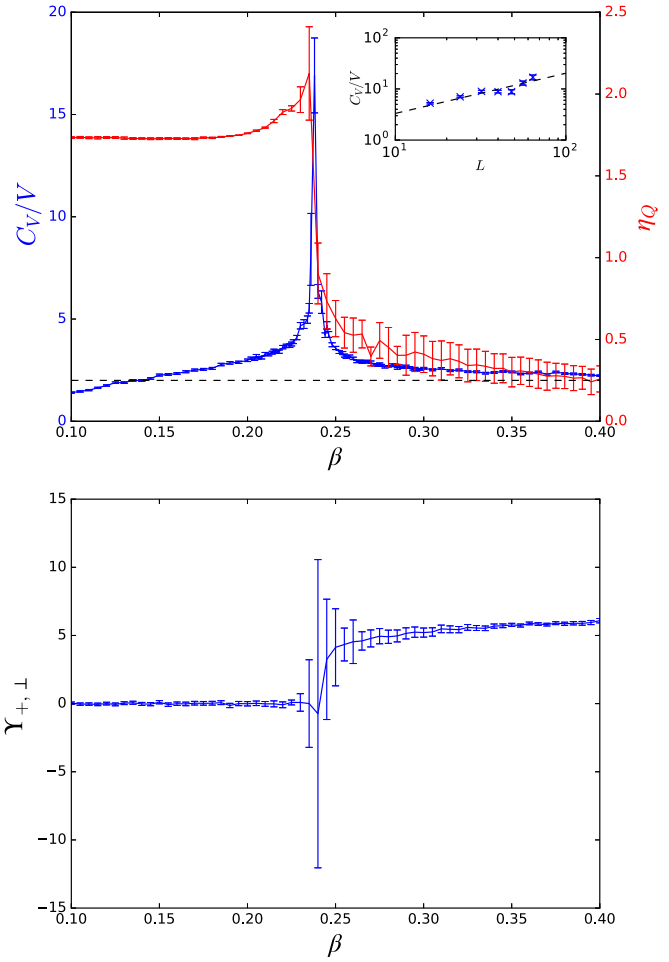

FIG. 11. Phase-sum structure function at the first Bragg peak, $\boldsymbol{Q}$, as a function of β for system sizes $L \in (16,24,32,40,48,56,64)$ as well as specific heat C_V/V for $L = 64$ (top) and helicity modulus of the phase-sum variable, $\Upsilon_{+,\perp}$ (bottom), at $\kappa = 1.0$ in the London limit. The inset of the top panel shows the scaling of the peak of the specific-heat curves for the same system sizes used in the structure function scaling. Note how the drop in the exponent $\eta_{\boldsymbol{Q}}$ as well as the jump in the helicity modulus both coincide with the sharp peak in the specific heat.

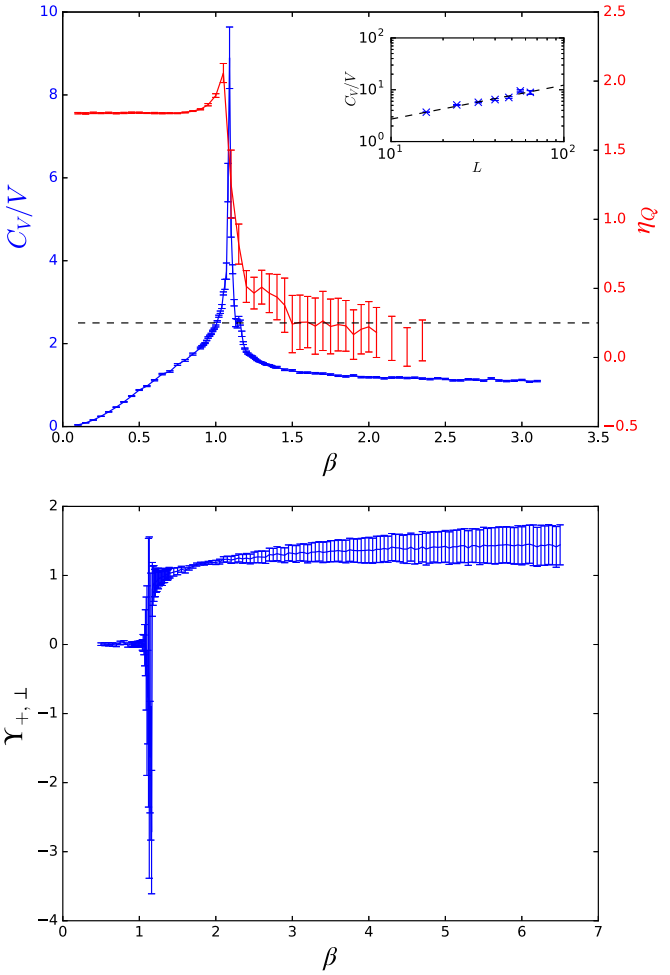

FIG. 12. Phase-sum structure function at the first Bragg peak, $\boldsymbol{Q}$, as a function of β for system sizes $L \in (16,24,32,40,48,56,64)$ as well as specific heat C_V/V for $L = 64$ (top), and the helicity modulus of the phase-sum variable, $\Upsilon_{+,\perp}$ (bottom), at $\kappa = 1.0$ in the London limit. The inset of the top panel shows the scaling of the peak of the specific-heat curves for the same system sizes used in the structure function scaling. Note how the drop in the exponent $\eta_{\boldsymbol{Q}}$ as well as the jump in the helicity modulus both coincide with the sharp peak in the specific heat.

The fact that we observe such a large and strongly scaling peak in Figs. 11(a) and 12(a) rules out a KT transition almost immediately. The similar behaviors between the two cases of Figs. 11 and 12 suggest that the London model is in fact a good effective model for this particular transition. We believe the main reason for the pinning is the periodic boundary conditions applied to the model. This biases the stripes to connect with themselves at the boundaries of the system, which in turn causes very slow equilibration at the critical point, as evident in the large error bars, especially of the helicity modulus. In particular, fluctuations associated with shifting or rotating the stripe configurations is particularly hard to resolve in the Monte Carlo simulations, as these are large-scale movements, which in turn are made even more difficult to resolve with periodic boundary conditions applied.

In an attempt to reduce the pinning effects present in Figs. 11 and 12 and to confirm their origin, we alter the model slightly. Instead of taking the London limit with $|\psi_{\boldsymbol{r},i}| = 1 \; \forall \, \boldsymbol{r},i$, we define a Thomas-Fermi trap that decouples the stripes from the boundaries of the system. Specifically, we set

$$|\psi_{\boldsymbol{r},i}| = \begin{cases} 1 - \left(\frac{r}{R}\right)^4, & r < R, \\ 0, & r > R. \end{cases} \tag{29}$$

However, this comes at the cost of not having a well-defined helicity modulus. This is the case for this particular model, as the decoupling of the stripes from the system boundary is the same as applying open boundary conditions. The helicity modulus relies on calculating the free-energy difference between the system with periodic boundary conditions and the system where an infinitesimal twist is applied to the phases at the boundary [51,52]. The simulation results of the London model in a Thomas-Fermi potential are shown in Fig. 13. Here we show only the scaling of the first-order peak in the phase

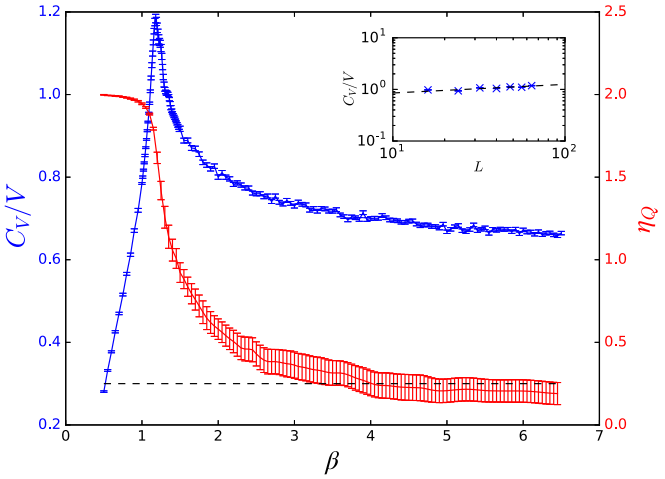

FIG. 13. Specific heat C_V/V (left axis) and the exponent $\eta_{\boldsymbol{Q}}$ (right axis). The inset shows a finite-size scaling of the peak of the specific heat for system sizes $L \in (16,24,32,40,48,56,64)$ at $\kappa = 1.0$ in the London limit with a Thomas-Fermi potential applied. The full specific-heat curve shown in the main panel is for the largest system sizes simulated, $L = 64$. Note how the peak of the specific-heat curves coincides with the jump in the exponent $\eta_{\boldsymbol{Q}}$.

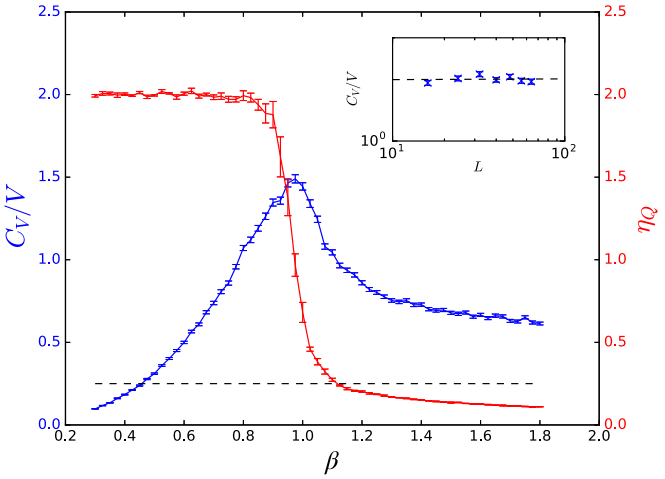

FIG. 14. Finite-size scaling of the height of the $\boldsymbol{q} = \boldsymbol{0}$ peak of the structure function calculated in an XY model. System sizes $L \in (16,24,32,40,48,56,64)$ have been used. The exponent grows linearly with temperature to the predicted value of $1/4$ (represented by the dotted line) at the critical temperature of the KT transition, $\beta_{\mathrm{KT}} \approx 1.12$.

sum structure function and the specific heat. Figure 13 shows that the signs of pinning that we are able to examine, namely the sharp peak of the specific heat and the sharp drop of $\eta_{\boldsymbol{Q}}$, are greatly reduced when the Thomas-Fermi potential is present. The specific-heat curve still shows a peak that coincides with the onset of scaling in the structure function, but the height and sharpness of the peak are reduced. We also find the peak to still exhibit scaling, with an exponent 0.17(4), as shown in the inset of Fig. 13. Without the helicity modulus, we are unable to determine confidently the nature of the phase transition, but it is evident that the signs of pinning are almost removed. In all likelihood, the remaining pinning signatures are associated with the aforementioned difficulty of moving or rotating entire stripe configurations, and they will disappear in the continuum limit.

As a comparison, we show results for the specific heat and the exponent $\eta_{\boldsymbol{Q}}$ taken from a simulation of the 2D XY model in Fig. 14. Here the exponent is measured by performing a finite-size scaling of the height of the $\boldsymbol{q} = \boldsymbol{0}$ peak in the phase-structure function. The defining characteristic that shows that this is a KT transition is the fact that the exponent $\eta_{\boldsymbol{Q}}$ reaches the limiting value of $1/4$ exactly at the KT-transition temperature, $\beta_{\mathrm{KT}} \approx 1.12$. We also show the scaling of the specific-heat peak, which has an exponent of 0 within the errors of our simulation.

Comparing the three different models of Figs. 11–13, we may conclude that the thermal transition from region I of the phase diagram shown in Fig. 10 into the disordered phase is a transition from a modulated two-dimensional superfluid phase into a normal fluid state. The transition has strong depinning characteristics when we apply periodic boundary conditions. These characteristics weaken and we approach a transition consistent with a KT-transition when we remove the periodic boundary conditions, but we are not able to rigorously characterize the transition as such due to the lack of a well-defined helicity modulus.

VI. CONCLUSIONS

We have studied a model of an imbalanced two-component Bose-Einstein condensate, with and without spin-orbit coupling in two spatial dimensions, including density-density interactions among the components. Specifically, we have examined the modulations in the phase texture of the complex order-parameter components induced by the spin-orbit coupling, its disordering and suppression by thermal fluctuations and interaction effects, as well as the modulations of the amplitude texture induced by a subtle interplay between spin-orbit and intercomponent interactions. We also examined the phase transitions of the model in the parameter regime where SOC is absent.

In the absence of SOC, we found that the phase transition of the model is in the KT universality class for all values of the intercomponent interaction strength we have considered. Here we observed a KT transition in the nonsuppressed superfluid condensate. These conclusions are made based on finite-size scaling of the helicity modulus at the transition point, as well as extrapolation of the negative dip of the fourth-order modulus to a nonzero value in the thermodynamic limit. Both methods strongly indicate a discontinuous jump in the superfluid density at the critical temperature.

In the presence of SOC, we observed a phase-modulated ground state at finite momenta in Monte Carlo simulations. When the intercomponent interactions are weaker than the intracomponent interactions, we find that the condensate occupies a single minimum at finite momentum, in agreement with previous works. This manifests itself as a modulation of the phases of the condensate ordering fields. For sufficiently strong intercomponent interactions and intermediate spin-orbit interactions, we observed that the spin-orbit induced

modulation is completely suppressed in favor of a completely imbalanced condensate. For strong spin-orbit coupling and sufficiently strong intercomponent interactions, however, the total interaction energy is minimized by keeping the phase modulation and introducing an additional, staggered modulation of the amplitudes with the same period. In this phase, we observe that the condensate occupies two q-vectors of equal magnitude but opposite alignment.

Finally, we examined the thermal phase transition of the spin-orbit-induced plane-wave modulated superfluid ground state into the normal fluid state in the London approximation. We show that the inclusion of periodic boundary conditions introduces a strong pinning effect, which weakens as we decouple the stripes from the edges of the system by applying a Thomas-Fermi potential. In the presence of the potential, we see signs of a Kosterlitz-Thouless transition, but we are not able to confirm this.

ACKNOWLEDGMENTS

We thank Egor Babaev for useful discussions. P.N.G. was supported by NTNU and the Research Council of Norway. A.S. was supported by the Research Council of Norway, through Grants No. 205591/V20 and No. 216700/F20, as well as European Science Foundation COST Action MPI1201. This work was also supported through the Norwegian consortium for high-performance computing (NOTUR).

APPENDIX: CLASSIFICATION OF THE KT TRANSITION

The defining characteristic of a Kosterlitz-Thouless transition is the universal jump of $2/(\pi\beta_c)$ of the superfluid density at the critical temperature, in the thermodynamic limit. Consider the free energy, where the phase of component i is twisted by an infinitesimal factor along the μ direction, $F(\Delta_{i,\mu})$. Technically, this amounts to replacing the phase of component i by a twisted phase,

$$\theta_{i,\mathbf{r}} \to \theta_{i,\mathbf{r}} - r_\mu \Delta_{i,\mu}. \tag{A1}$$

The superfluid density, or helicity modulus, is the second derivative of the free energy with respect to the twist,

$$\langle \Upsilon_{i,\mu} \rangle \equiv \frac{1}{V} \frac{\partial^2 F(\Delta_{i,\mu})}{\partial \Delta_{i,\mu}^2}. \tag{A2}$$

Similarly, the fourth-order modulus is the fourth derivative of the free energy with respect to the twist,

$$\langle \Upsilon_{4,i,\mu} \rangle \equiv \frac{1}{V^2} \frac{\partial^4 F(\Delta_{i,\mu})}{\partial \Delta_{i,\mu}^4}. \tag{A3}$$

Derivatives of odd order vanish due to symmetry.

In terms of amplitudes and phases of the Ginzburg-Landau theory for a two-component condensate, the helicity modulus is

$$V\langle \Upsilon_{i,\mu} \rangle = \langle c_{i,\mu} \rangle - \beta \langle s_{i,\mu}^2 \rangle, \tag{A4}$$

while the fourth-order modulus is

$$V^2\langle \Upsilon_{4,i,\mu} \rangle = -3V^2\beta \langle (\Upsilon_{i,\mu} - \langle \Upsilon_{i,\mu} \rangle)^2 \rangle - 4V\langle \Upsilon_{i,\mu} \rangle + 3\langle c_{i,\mu} \rangle + 2\beta^3 \langle s_{i,\mu}^4 \rangle, \tag{A5}$$

where we have defined

$$c_{i,\mu} \equiv \sum_{\mathbf{r}} |\psi_{i,\mathbf{r}+\boldsymbol{\mu}}||\psi_{i,\mathbf{r}}| \cos(\theta_{i,\mathbf{r}+\boldsymbol{\mu}} - \theta_{i,\mathbf{r}}), \tag{A6}$$

$$s_{i,\mu} \equiv \sum_{\mathbf{r}} |\psi_{i,\mathbf{r}+\boldsymbol{\mu}}||\psi_{i,\mathbf{r}}| \sin(\theta_{i,\mathbf{r}+\boldsymbol{\mu}} - \theta_{i,\mathbf{r}}). \tag{A7}$$

This is similar to the expressions obtained when considering a 2D XY model. The amplitude fluctuations only influence the moduli indirectly by weighting the terms in the sums. Hence, the moduli of each component are coupled indirectly through the potential.

At the critical temperature, the helicity modulus is expected to scale as

$$\Upsilon_{i,\mu}(L) = \Upsilon(\infty)\left(1 + \frac{1}{2}\frac{1}{\log L + C}\right) \tag{A8}$$

with system size [45]. We fit the data at finite size for different values of β, and we determine at which β the best fit is obtained by using the Anderson-Darling test statistic. This allows an extrapolation of the value of the jump, $\Upsilon(\infty)$, which may be compared to the KT prediction. This will also result in an estimate of the critical temperature.

By considering an expansion of the free energy in terms of the phase twist,

$$F(\Delta_{i,\mu}) - F(0) = \langle \Upsilon_{i,\mu} \rangle \frac{\Delta_{i,\mu}^2}{2} + \langle \Upsilon_{4,i,\mu} \rangle \frac{\Delta_{i,\mu}^4}{4!}. \tag{A9}$$

For the system to be stable, the change in the free energy has to be greater than or equal to zero. If $\Upsilon_{4,i,\mu}$ is finite and negative in the thermodynamic limit at the critical temperature, $\Upsilon_{i,\mu}$ cannot go continuously to zero at the critical temperature [46]. Therefore, by calculating the negative dip in the fourth-order modulus for increasing system size, a finite value as $L \to \infty$ signals a discontinuous jump in the helicity modulus. Furthermore, the temperature at which the dip is located should converge to the critical temperature. Extrapolation of the location of the dip may therefore be compared to the above estimate of the critical temperature, as an additional consistency check. However, this convergence is generally quite slow.

[1] Y. K. Kato, R. C. Myers, A. C. Gossard, and D. D. Awschalom, Science **306**, 1910 (2004).
[2] M. Konig, Science **318**, 766 (2007).
[3] C. L. Kane and E. J. Mele, Phys. Rev. Lett. **95**, 146802 (2005).
[4] B. A. Bernevig, T. L. Hughes, and S.-C. Zhang, Science **314**, 1757 (2006).
[5] D. Hsieh *et al.*, Nature (London) **452**, 970 (2008).
[6] M. Z. Hasan and C. L. Kane, Rev. Mod. Phys. **82**, 3045 (2010).
[7] J. D. Koralek, Nature (London) **458**, 610 (2009).
[8] Y.-J. Lin, K. Jimenez-Garcia, and I. B. Spielman, Nature (London) **471**, 83 (2011).
[9] V. Galitski and I. B. Spielman, Nature (London) **494**, 49 (2013).

[10] Y. A. Bychkov and E. I. Rashba, J. Phys. C **17**, 6039 (1984).
[11] G. Dresselhaus, Phys. Rev. **100**, 580 (1955).
[12] C. J. Myatt, E. A. Burt, R. W. Ghrist, E. A. Cornell, and C. E. Wieman, Phys. Rev. Lett. **78**, 586 (1997).
[13] D. S. Hall, M. R. Matthews, J. R. Ensher, C. E. Wieman, and E. A. Cornell, Phys. Rev. Lett. **81**, 1539 (1998).
[14] G. Modugno, M. Modugno, F. Riboli, G. Roati, and M. Inguscio, Phys. Rev. Lett. **89**, 190404 (2002).
[15] D. J. McCarron, H. W. Cho, D. L. Jenkin, M. P. Köppinger, and S. L. Cornish, Phys. Rev. A **84**, 011603 (2011).
[16] P. Wang, Z.-Q. Yu, Z. Fu, J. Miao, L. Huang, S. Chai, H. Zhai, and J. Zhang, Phys. Rev. Lett. **109**, 095301 (2012).
[17] I. Bloch, Nat. Phys. **1**, 23 (2005).
[18] C. Hamner, Y. Zhang, M. A. Khamehchi, M. J. Davis, and P. Engels, Phys. Rev. Lett. **114**, 070401 (2015).
[19] J. Struck, J. Simonet, and K. Sengstock, Phys. Rev. A **90**, 031601 (2014).
[20] C. J. Kennedy, G. A. Siviloglou, H. Miyake, W. C. Burton, and W. Ketterle, Phys. Rev. Lett. **111**, 225301 (2013).
[21] A. P. Schnyder, S. Ryu, A. Furusaki, and A. W. W. Ludwig, Phys. Rev. B **78**, 195125 (2008).
[22] A. Kitaev, in *Periodic Table for Topological Insulators and Superconductors*, edited by V. Lebedev and M. Feigel'man, AIP Conf. Proc. No. 1134 (AIP, New York, 2009), p. 22.
[23] X.-L. Qi, T. L. Hughes, S. Raghu, and S.-C. Zhang, Phys. Rev. Lett. **102**, 187001 (2009).
[24] T. Graß, K. Saha, K. Sengupta, and M. Lewenstein, Phys. Rev. A **84**, 053632 (2011).
[25] W. S. Cole, S. Zhang, A. Paramekanti, and N. Trivedi, Phys. Rev. Lett. **109**, 085302 (2012).
[26] J. Radić, A. Di Ciolo, K. Sun, and V. Galitski, Phys. Rev. Lett. **109**, 085303 (2012).
[27] D. Toniolo and J. Linder, Phys. Rev. A **89**, 061605 (2014).
[28] T. D. Stanescu, B. Anderson, and V. Galitski, Phys. Rev. A **78**, 023616 (2008).
[29] S.-K. Yip, Phys. Rev. A **83**, 043616 (2011).
[30] K. Kasamatsu, Phys. Rev. A **92**, 063608 (2015).
[31] R. Barnett, S. Powell, T. Graß, M. Lewenstein, and S. Das Sarma, Phys. Rev. A **85**, 023615 (2012).
[32] T. Ozawa and G. Baym, Phys. Rev. Lett. **109**, 025301 (2012).
[33] L. Radzihovsky, Phys. Rev. A **84**, 023611 (2011).
[34] G. Ceccarelli, J. Nespolo, A. Pelissetto, and E. Vicari, Phys. Rev. A **93**, 033647 (2016).
[35] J. Smiseth, E. Smørgrav, E. Babaev, and A. Sudbø, Phys. Rev. B **71**, 214509 (2005).
[36] D. V. Fil and S. I. Shevchenko, Phys. Rev. A **72**, 013616 (2005).
[37] E. K. Dahl, E. Babaev, and A. Sudbø, Phys. Rev. B **78**, 144510 (2008).
[38] C. Wang, C. Gao, C.-M. Jian, and H. Zhai, Phys. Rev. Lett. **105**, 160403 (2010).
[39] T. A. Sedrakyan, A. Kamenev, and L. I. Glazman, Phys. Rev. A **86**, 063639 (2012).
[40] N. Metropolis, A. W. Rosenbluth, M. N. Rosenbluth, A. H. Teller, and E. Teller, J. Chem. Phys. **21**, 1087 (1953).
[41] W. K. Hastings, Biometrika **57**, 97 (1970).
[42] M. Matsumoto and T. Nishimura, ACM Trans. Model. Comput. Simul. **8**, 3 (1998).
[43] A. M. Ferrenberg and R. H. Swendsen, Phys. Rev. Lett. **63**, 1195 (1989).
[44] B. A. Berg, Comput. Phys. Commun. **69**, 7 (1992).
[45] H. Weber and P. Minnhagen, Phys. Rev. B **37**, 5986 (1988).
[46] P. Minnhagen and B. J. Kim, Phys. Rev. B **67**, 172509 (2003).
[47] E. B. Stiansen, I. B. Sperstad, and A. Sudbø, Phys. Rev. B **85**, 224531 (2012).
[48] E. V. Herland, E. Babaev, P. Bonderson, V. Gurarie, C. Nayak, and A. Sudbø, Phys. Rev. B **85**, 024520 (2012).
[49] G. Ceccarelli, J. Nespolo, A. Pelissetto, and E. Vicari, Phys. Rev. B **88**, 024517 (2013).
[50] J. M. Kosterlitz, J. Phys. C **7**, 1046 (1974).
[51] M. E. Fisher, M. N. Barber, and D. Jasnow, Phys. Rev. A **8**, 1111 (1973).
[52] Y.-H. Li and S. Teitel, Phys. Rev. B **47**, 359 (1993).